A threedimensional, quantum mechanical study of exchange and charge transfer processes in the (Ar+H2)+ system

Michael Baer and Hiroki Nakamura

Citation: The Journal of Chemical Physics **87**, 4651 (1987); doi: 10.1063/1.452828
View online: http://dx.doi.org/10.1063/1.452828
View Table of Contents: http://scitation.aip.org/content/aip/journal/jcp/87/8?ver=pdfcov
Published by the AIP Publishing

A three-dimensional, quantum mechanical study of exchange and charge transfer processes in the $(Ar+H_2)^+$ system

Michael Baer
Soreq Nuclear Research Center, Yavne 70600, Israel

Hiroki Nakamura
Division of Theoretical Studies, Institute for Molecular Science, Myodaiji, Okazaki 444, Japan

(Received 13 April 1987; accepted 19 June 1987)

A three-dimensional quantum mechanical study of the $(Ar + H_2)^+$ system was carried out within the reactive infinite order sudden approximation. All three arrangement channels for exchange and charge transfer were treated simultaneously. Steric factors, opacity functions, angular distributions, and integral cross sections were calculated. Whenever possible, these were compared with both experimental and trajectory surface hopping (TSH) results. Whereas the fit with the TSH results was reasonable, the fit obtained with the experiment was less satisfactory. The reason for that can be attributed at least partially to the semiempirical DIM potential employed in the calculation.

I. INTRODUCTION

For the last few years research in molecular dynamics has been characterized by the close interaction between experiment and theory. A study of a particular system or certain features thereof may be initiated by a theoretical group or an experimental laboratory but then the efforts of both must be combined to elucidate the underlying mechanisms of the dynamic processes.

One of the most exciting areas of research within molecular dynamics is that of the exchange atom–diatom processes. This is because the detailed mechanism of these exchange processes is still an open question. The emphasis in this area was put on interactions between neutrals and not between ions for two main reasons: (a) Reactions between neutrals are more frequent than between ions and (b) theoretically, treating reactions between neutrals seems easier. However, the experimental study of ion–molecule reactions is, to a certain extent, more convenient than the study of reactions between neutrals because (a) the reagents can be prepared with any well-defined translational energy and (b) the products can be easily detected. Since under these circumstances the experimental results are quite reliable, various theories can be examined more confidently and relevant models can be devised. As examples we refer to the Langevin formula for the rate constant[1] and to improved versions of that approach,[2] to classical[2(a),3] and quantum mechanical approximate treatments,[4] and to the spectator stripping model to determine final energy distribution.[5–7]

$(Ar + H_2)^+$ is considered to be a prototype system to study the competition between chemical reaction and charge transfer in ion–molecule collisions. As an entrance channel we may have either $Ar^+ + H_2$ or $Ar + H_2^+$, both of which lead, upon reaction, to the ArH^+ ion:

$$Ar^+ + H_2 \rightarrow ArH^+ + H; \quad \Delta E = -1.61 \text{ eV} \qquad \text{(Ia)}$$

and

$$Ar + H_2^+ \rightarrow ArH^+ + H; \quad \Delta E = -1.30 \text{ eV}. \qquad \text{(Ib)}$$

Charge transfer takes place only in the entrance channel:

$$Ar^+ + H_2 \rightarrow Ar + H_2^+; \quad \Delta E = -0.31 \text{ eV} \qquad \text{(Ic)}$$

and

$$Ar + H_2^+ \rightarrow Ar^+ + H_2; \quad \Delta E = +0.31 \text{ eV}. \qquad \text{(Id)}$$

This system has been exposed to a large number of experimental studies and although the most advanced experimental techniques were used, different and sometimes contadictory results were obtained in various laboratories. At this stage we shall distinguish between two kinds of studies—those devoted to integral cross sections and those to differential cross sections. As for the first group, the most detailed studies were carried out by Tanaka *et al.*,[8,9] who used their reliable TESICO technique to study all four processes mentioned above as a function of translational energy and initial vibrational state and as a function of the initial spin state of Ar^+. The other studies concentrated on either one type of reagents or the other. Namely, whereas Lacmann and Henglein,[10] Amme and McIlwain,[11] and Ervin and Armentrout[12] studied the $Ar^+ + H_2(D_2)$, Chupka and Russel,[13] Campbell *et al.*[14] and, most recently, Houle *et al.*[15] studied the $Ar + H_2^+$ system. Differential cross sections were measured by Hierl *et al.*[16] for reaction (Ic) and by Billola *et al.*[17,18] for reactions (Ib) and (Id), respectively. As for theoretical research, only a few studies were performed. Using the DIM potential constructed by Kuntz and Roach,[19] Chapman and Preston[20] carried out the first dynamic studies on this system. Employing the trajectory surface hopping (TSH) method, they calculated the cross sections for the two competing processes with $Ar^+ + H_2$ as reagents. Later, Baer and Beswick[21,22] carried out a full quantum mechanical study for the collinear arrangement, in which all four processes were treated at once, employing the method developed by Top and Baer.[23] Certain aspects of the stripping mechanism for $Ar^+ + H_2$ were studied quantum mechanically by Yuan and Micha.[24] Recently, Chapman[25] performed another TSH study on this system. This time she not only considered all four reactions, but also carried out the calculations as a function of initial vibrational state and initial translational energy.

 0021-9606/87/204651-14$02.10

We describe here a three-dimensional quantum mechanical study of the $(Ar + H_2)^+$ system within the reactive infinite order sudden approximation (RIOSA).[26–29] For this study, we extended the RIOSA, which was originally devised for a single surface system, to treat a multisurface problem.

The RIOSA is characterized by two basic features (which, in fact, enable a quantum mechanical three-dimensional treatment of any atom–diatom system): (a) The numerical treatment in each arrangement channel is performed by holding the corresponding γ angle constant. Thus for the entrance (reagents) channel (A,BC) (see Fig. 1) the angle γ_i is kept constant, and in the exit (products) channel (AB,C) the angle γ_f is kept constant.[27,29] In this way, all S matrix elements become parametrically dependent on these two angles. (b) Within the RIOSA a one-to-one mapping between γ_i and γ_f is devised.[27,29] Thus the S matrix elements are, in fact, dependent on one angle only, namely γ_i. To obtain the physical magnitudes of interest weighted integrations over γ_i are carried out (see Sec. IV).

In this work we shall refer to the following six reactions:

$$Ar + H_2^+(v_i = 0) \rightarrow \begin{cases} ArH^+ + H; & \Delta E = -1.315 \text{ eV} \quad \text{(IIa)} \\ Ar^+ + H_2; & \Delta E = 0.298 \text{ eV} \quad \text{(IIb)} \end{cases}$$

$$Ar + H_2^+(v_i = 1) \rightarrow \begin{cases} ArH^+ + H; & \Delta E = -1.593 \text{ eV} \quad \text{(IIc)} \\ Ar^+ + H_2; & \Delta E = 0.020 \text{ eV} \quad \text{(IId)} \end{cases}$$

$$Ar^+ + H_2(v_i = 0) \rightarrow \begin{cases} ArH^+ + H; & \Delta E = -1.613 \text{ eV} \quad \text{(IIe)} \\ Ar + H_2^+; & \Delta E = -0.298 \text{ eV} \quad \text{(IIf)} \end{cases}$$

Within the present study the ΔE values given here were derived from the DIM potentials.[19] Because of its complexity, the numerical treatment was carried out for only one total energy value, i.e., $E_{tot} = 0.6$ eV.

II. THE POTENTIAL

The DIM surfaces employed to perform the study were as given by Kuntz and Roach[19] and slightly modified by Chapman.[25] Six $^2A'$ surfaces arising from the atomic ground states of (Ar^+,H,H) and (Ar,H^+,H) were included in the calculations. Since spin–orbit coupling was neglected the energy of $Ar^+(^2P)$, i.e., E_{Ar^+}, was taken as

$$E_{Ar^+} = \tfrac{1}{3}[2E_{Ar^+}(^2P_{3/2}) + E_{Ar^+}(^2P_{1/2})]. \quad (1)$$

Whereas the reactive process takes place on the lowest adiabatic surface only, the charge transfer process takes place among the three lowest surfaces, the lowest of which correlates with $Ar^+ + H_2$ and the other two with $Ar^+ + H_2$. However, it has been established by Chapman and Preston[20] that only one of these two surfaces interacts with the lowest one at one time. Since in our and in the TSH treatments only two surfaces are considered, a scheme was worked out which yields the two interacting surfaces at one time, although all three are taken into account.[20,25]

The selection is done as follows: One surface, which is always included, is the lowest eigenvalue of the DIM matrix. The second surface chosen is one of the two next lowest eigenvalues of the DIM matrix that most (nonadiabatically) couples to the lowest surface (the nonadiabatic coupling between the two surfaces themselves is usually negligibly small). The procedure for determining the strength of the nonadiabatic coupling terms has been described in detail elsewhere[25] but will be briefly repeated here, for the sake of completeness.

The potential energy surfaces and the corresponding nonadiabatic coupling terms as obtained from the DIM matrix have two important features:

(1) For energies of chemical interest ($E_{tot} \leq 5$ eV), the interactions between the lowest and the other adiabatic surfaces take place in the entrance $(Ar + H_2^+; Ar^+ + H_2)$ arrangement channel only.

(2) Of the three different kinds of nonadiabatic coupling terms, i.e., $(t_{r_1}^{(1)})_{ij}$, $(t_{r_2}^{(1)})_{ij}$, $(t_{r_3}^{(1)})_{ij}$ where i and j designate the surfaces and r_1, r_2, and r_3 are interatomic distances, only $(t_{r_2}^{(1)})_{ij}$, where $r_2 = r_{H-H}$ is large and the other two are much smaller.

These two features make it easier to carry out the required search. Thus instead of considering the whole configuration space we concentrate on the entrance channel only and we determine the strength of the nonadiabatic coupling between the lowest and the next two adiabatic surfaces according to the size of $(t_{r_2}^{(1)})_{12}$ and $(t_{r_2}^{(1)})_{13}$.

It was found, that in the entrance channel the two coupling terms fulfill the following relations:

$$\begin{aligned} &(t_{r_2}^{(1)})_{12} \gg (t_{r_2}^{(1)})_{13} \quad \text{for} \quad r_2 > 1.7 \text{ a.u.}, \\ &(t_{r_2}^{(1)})_{12} \ll (t_{r_2}^{(1)})_{13} \quad \text{for} \quad r_2 > 1.7 \text{ a.u.} \end{aligned} \quad (2)$$

These relations hold except in the vicinity of $r = 1.7$ a.u. where $(t_{r_2}^{(1)})_{12}$ and $(t_{r_2}^{(1)})_{13}$ are almost equal.

As a result of these features the two interacting surfaces in the entrance channel are

$$V_1(r_1,r_2,r_3) = U_1(r_1,r_2,r_3), \quad (3a)$$

$$V_2(r_1,r_2,r_3) = \begin{cases} U_2(r_1,r_2,r_3) & \text{for } r_2 > 1.7 \text{ a.u.} \\ U_3(r_1,r_2,r_3) & \text{for } r_2 < 1.7 \text{ a.u.} \end{cases}, \quad (3b)$$

where $U_i(r_1,r_2,r_3) i = 1,2,3$ are the three lowest eigenvalues of the DIM matrix. Consequently the nonadiabatic coupling terms used are

$$(\tau_{r_2}^{(1)})_{12} = \begin{cases} (t_{r_2}^{(1)})_{12} & \text{for } r_2 > 1.7 \text{ a.u.} \\ (t_{r_2}^{(1)})_{13} & \text{for } r_2 < 1.7 \text{ a.u.} \end{cases}. \quad (4)$$

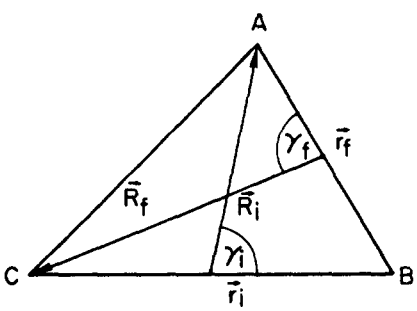

FIG. 1. The three-atom system: (A,BC) is the reagents channel with coordinates (R_i,r_i,γ_i) and (AB,C) is the products channel with the coordinates (R_f,r_f,γ_f).

Having defined the adiabatic surfaces (see Fig. 2) and the nonadiabatic coupling terms one could, in principle, treat the scattering problem. However, for numerical instability reasons it is necessary to transform from the adiabatic to the diabatic framework. This general procedure has been described elsewhere[30] but since in the present study it is implemented within the RIOSA we shall briefly go over it in the next section.

III. THE ADIABATIC–DIABATIC TRANSFORMATION WITHIN THE FRAMEWORK OF THE RIOSA

The IOSA and likewise the RIOSA are approximations of fixed angle dynamics. The characteristic IOSA angle is defined as

$$\gamma = \cos^{-1}(\hat{\mathbf{R}}\cdot\hat{\mathbf{r}}), \tag{5}$$

where **R** and **r** are the translational and vibrational vectors. Within the RIOSA one distinguishes between two such angles, one for the reagents and the other for the products (see Fig. 1). However, the nonadiabatic coupling takes place only in the reagents channel, so we have to consider only one IOSA angle. Consequently the adiabatic–diabatic transformation must be described for a given angle γ. This approach is justifiable due to the fact that the angular nonadiabatic coupling resulting from variation in γ is relatively small as compared to the vibrational nonadiabatic coupling.

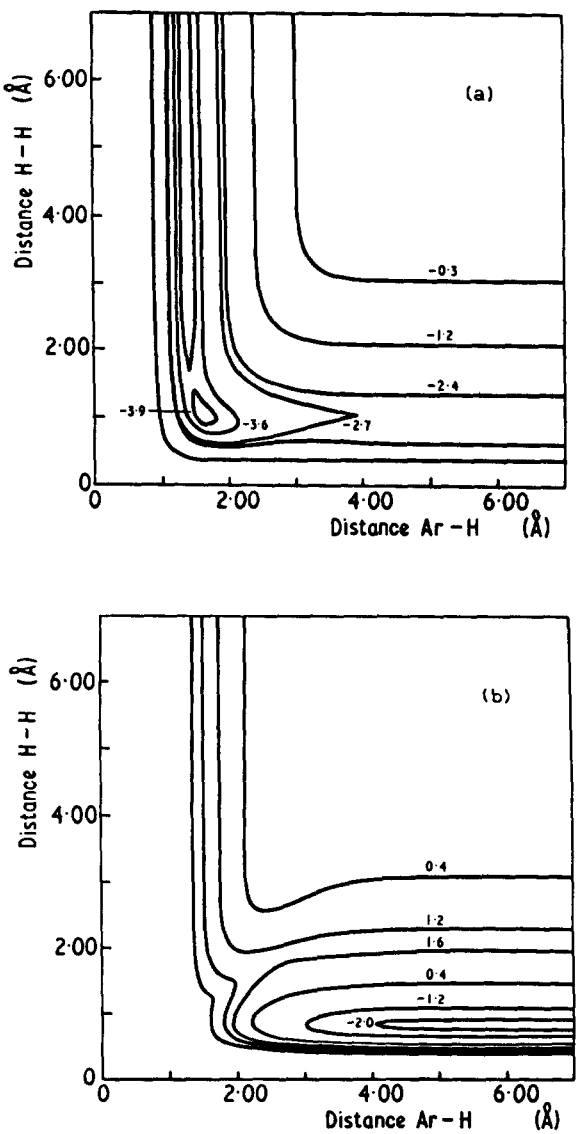

FIG. 2. The potential energy surfaces as a function of interatomic distances $r_{Ar\text{-}H}$ and $r_{H\text{-}H}$ (numbers stand for energies in eV): (a) the lowest adiabatic surface; (b) the second adiabatic surface.

Thus the following two nonadiabatic coupling terms, the translational coupling $\tau_R^{(1)}(R,r;\gamma)$ and the vibrational coupling $\tau_r^{(1)}(R,r;\gamma)$, are given, as are the two corresponding adiabatic surfaces $V_1(R;r;\gamma)$ and $V_2(R,r;\gamma)$. Consequently, the two corresponding diabatic surfaces $W_i(R,r;\gamma); i = 1,2$ and the diabatic coupling term $W_{12}(R,r;\gamma)$ are given as[30]

$$W_1 = \cos^2\alpha V_1 + \sin^2\alpha V_2, \tag{6a}$$

$$W_2 = \sin^2\alpha V_1 + \cos^2\alpha V_2, \tag{6b}$$

$$W_{12} = \tfrac{1}{2}\sin 2\alpha(V_2 - V_1), \tag{6c}$$

where the angle $\alpha = \alpha(R,r;\gamma)$ is calculated from the line integral

$$\alpha = \alpha_0 + \int_{R_0}^{R} \tau_R^{(1)}(R,r_0;\gamma)dR + \int_{r_0}^{r} \tau_r^{(1)}(R;r;\gamma)dr. \tag{7}$$

Here $\alpha_0 = \alpha(R_0,r_0;\gamma)$ is assumed to be given.

The translational and vibrational nonadiabatic coupling terms $\tau_R^{(1)}$ and $\tau_r^{(1)}$ are calculated from the ordinary interatomic nonadiabatic coupling terms $\tau_{r_i}^{(1)}$: $i = 1,2,3$, employing the chain rule. Thus

$$\tau_x^{(1)} = \sum_{i=1}^{3} \tau_{r_i}^{(1)} \frac{\partial r_i}{\partial x}; \quad x = R,r. \tag{8}$$

Recalling the relations

$$r_1^2 = R^2 + \tfrac{1}{4}r^2 - rR\cos\gamma, \tag{9a}$$

$$r_2 = r, \tag{9b}$$

$$r_3^2 = R^2 + \tfrac{1}{4}r^2 + rR\cos\gamma, \tag{9c}$$

we get for the general case,

$$\tau_R^{(1)} = \frac{R - \frac{1}{2}r\cos\gamma}{r_1}\tau_{r_1}^{(1)} + \frac{R + \frac{1}{2}r\cos\gamma}{r_3}\tau_{r_3}^{(1)}, \tag{10a}$$

$$\tau_r^{(1)} = \frac{r - 2R\cos\gamma}{4r_1}\tau_{r_1}^{(1)} + \tau_{r_2}^{(1)} + \frac{r + 2R\cos\gamma}{4r_3}\tau_{r_3}^{(1)}. \tag{10b}$$

Here again r_2 is the interatomic distance between the two hydrogens.

The interatomic nonadiabatic coupling terms $\tau_{r_i}^{(1)}$; $i = 1,2,3$ were calculated employing the Hellmann and Feynman theorem.[30] Thus

$$\tau_P^{(1)} = \left[\mathbf{A}_1\left(\frac{\partial \mathbf{H}}{\partial P}\right)\mathbf{A}_2^*\right] \Big/ V_2 - V_1; \quad P = r_1,r_2,r_3, \tag{11}$$

where $\mathbf{A}_1$ and $\mathbf{A}_2$ are eigenvectors associated with the eigenvalues V_1 and V_2 respectively and **H** is the DIM matrix.

The angle α as a function of r for the collinear case, namely, for $\gamma = 0$, is shown in Fig. 3. Several curves are presented for different R values. The calculations were done in the reagents channel by assuming $\alpha_0 = 0$ at $R_0 = 5$ Å and $r_0 = 0.5$ Å.

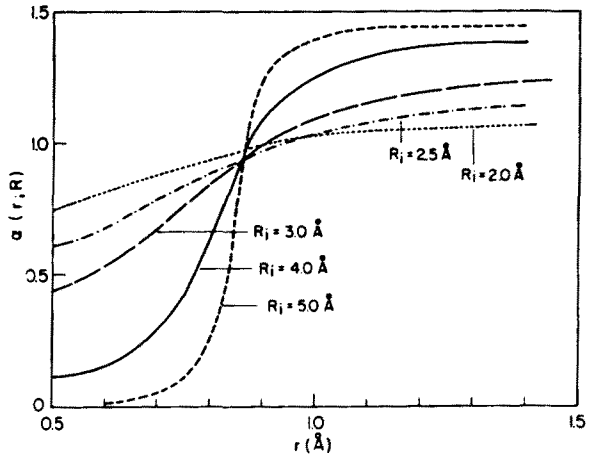

FIG. 3. The adiabatic–diabatic transformation angle $\alpha(r_i,R_i;\gamma_i=0)$ as a function of r_i for different values of R_i.

The following features are to be noticed:

(a) The range of variation of α is $0 \le \alpha \le \pi/2$.

(b) The rate of change of α with respect to r becomes larger as R gets larger, namely, the farther the calculations are carried out in the asymptotic region.

These features are expected from general considerations, but it is particularly important to notice how $\alpha(r,R;\gamma)$ approaches its asymptotic value, which can be shown to be

$$\lim_{R\to\infty} \alpha(R,r;\gamma) = \begin{cases} 0; & r < r_s \\ \pi/4; & r = r_s, \\ \pi/2; & r > r_s \end{cases} \tag{12}$$

where r_s is the intersection point between the H_2 and the H_2^+ potential curves.

Repeating these calculations for different IOSA angles γ, we find that $\tau^{(1)}(R,r;\gamma)$ is only slightly dependent on γ. Such a comparison is shown in Fig. 4, comparing values for $\gamma = 0$ and $\gamma = 60°$ (the range of variation for γ is $0 \le \gamma \le \pi/2$). The comparison is done for three values of R, i.e., $R = 2$, 3, 4 Å.

In order to reduce the amount of computation time, the angle α was fitted to an analytic function of the form

$$\alpha = \alpha_0 + \bar{\alpha}\{1 + \tanh[q(r - r_s)]\}. \tag{13}$$

Here α_0, $\bar{\alpha}$, q, and r_s are parameters that were derived by "trial and error" to determine an analytic α as close as possible to the calculated one. The values of α_0, $\bar{\alpha}$, and r_s as a function of R are shown in Fig. 5 and the value of q in Fig. 6. In Fig. 6 we also show the value of the nonadiabatic coupling term $\tau_r^{(1)}(r = r_s,R;\gamma = 0)$. For this magnitude we show two curves, one based on the exact treatment [Eqs. (10b) and (11)] and the other derived from the fit given in Eq. (13). As for the values calculated from the fit, we make use of the fact that

$$\frac{d\alpha}{dr} = \tau_r^{(1)}. \tag{14}$$

Consequently, Eq. (13) yields

$$\tau_r^{(1)}(r = r_s,R;\gamma) = \bar{\alpha}(R;\gamma)q(r;\gamma). \tag{15}$$

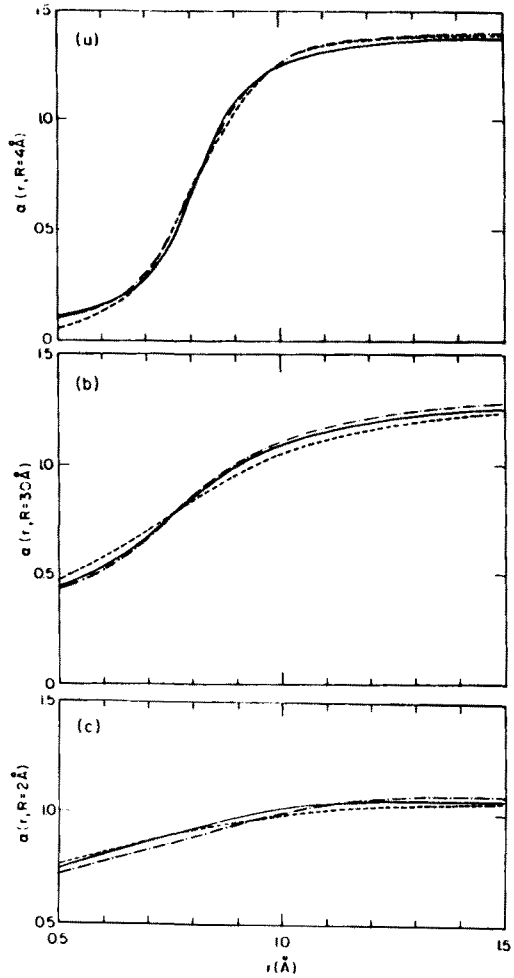

FIG. 4. The adiabatic–diabatic transformation angle $\alpha(r_i,R_i;\gamma_i)$ for different values of R_i. (a) $R_i = 4$ Å; (b) $R_i = 3$ Å; (c) $R_i = 2$ Å. — Exact collinear curve; --- fit according to Eq. (13); -·-·- exact curve for $\gamma_i = 60°$.

The comparison between the analytic fit of α [Eq. (13)] and the actual values is shown in Fig. 4. It is also seen that the same analytic presentation will apply for $\gamma = 60°$ and therefore we assumed throughout this study that α is given by Eq. (13) where the parameters for a given R value were deter-

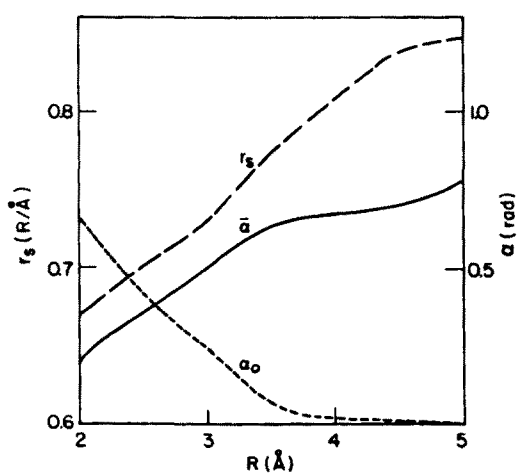

FIG. 5. The parameters $r_s(R_i)$, $\alpha_0(R_i)$, and $\bar{\alpha}(R_i)$ [see Eq. (13)] as a function of R_i. Note the two axes; one for r_s and the other for α_0 and $\bar{\alpha}$.

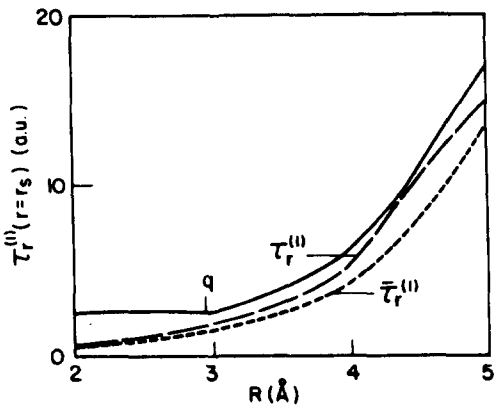

FIG. 6. The exact vibrational nonadiabatic coupling term $\tau_r^{(1)}(r_i = r_s, R_i; \gamma_i = 0)$, the parameter $q(R_i)$ [see Eq. (13)] and the approximated vibrational nonadiabatic coupling term $\bar{\tau}_r^{(1)} = \bar{\alpha}_q$ as a function of R_i.

mined by interpolation (or extrapolation). All parameters were assumed to be independent of the orientation angle γ.

The asymptotic behavior of α [cf. Eq. (12)] guarantees the correct asymptotic limit of the potential, namely it leads to the correct diatomic potentials:

$$W_1 \rightarrow \begin{cases} V_1 : r < r_s \\ V_2 : r > r_s \end{cases}, \tag{16}$$

$$W_2 \rightarrow \begin{cases} V_2 : r < r_s \\ V_1 : r > r_s \end{cases}, \tag{17}$$

and

$$W_{12} = W_{21} \rightarrow 0. \tag{18}$$

It is noticed that W_1 and W_2 are the potentials of H_2 and H_2^+, respectively.

IV. THE ADIABATIC PATH WITHIN THE DIABATIC REPRESENTATION

There are several reasons why it is desirable to transform from the adiabatic to the diabatic representation:

(a) The nonadiabatic coupling terms are often of an inconvenient form for numerical treatment. They can have sharp spikes (in the vicinity of the seam) or even become infinity, as was shown previously. Thus, the existence of such functions within a large set of coupled differential equations will cause a lot of numerical instabilities that eventually will inhibit the derivation of the correct solution.

(b) In many cases (and the present case is one of these) the asymptotic physical potential is given within the diabatic and not the adiabatic representation.

(c) Since within the adiabatic representation the differential equations contain explictly first order derivatives, this will enforce the diagonalization of a $2N \times 2N$ potential-type matrix instead of a $N \times N$ matrix as is the case in the diabatic representation.

Thus the transformation to the diabatic representation is fully justified. However, once the diabatic representation is reached, new difficulties are encountered. The diabatic potential energy matrices obtained from Eq. (6) sometimes turn out to have large off-diagonal terms which cause numerical approaches, including those based on diagonalization of the *close coupling* potential matrix, to be very unstable. Since, in general, there are many diabatic representations, it is desirable to find the one with the smallest possible off-diagonal terms, and consequently the diabatic surfaces become closely similar to the original adiabatic one. In order to achieve this we introduced the idea of the *adiabatic path* and we shall now discuss it to a certain extent.

Since within the IOSA only two "active" coordinates are encountered, namely R and r, we shall consider the following equation:

$$\nabla^2\psi + (\mathbf{W} - E)\psi = 0, \tag{19}$$

where $\mathbf{W} = \mathbf{W}(R,r;\gamma)$ is the 2×2 diabatic potential matrix [see Eqs. (6)] ψ is a two component wave function, and ∇^2 stands for

$$\nabla^2 = -\frac{\hbar^2}{2\mu}\left(\frac{\partial^2}{\partial R^2} + \frac{\partial^2}{\partial r^2}\right). \tag{20}$$

Here μ is a characteristic mass of the system. In order to solve such an equation one usually propagates along a translational coordinate R and one employs the close coupling expansion with respect to the vibrational coordinate r.

We introduce a path along the reaction coordinate, which is defined by the equation

$$r = r(R). \tag{21}$$

Our aim is to find a diabatic representation which will yield, for a certain number of points along the path $[R_i, r(R_i)]; i = 1,N$, a potential matrix $\bar{\mathbf{W}}$ which is diagonal. In other words, we are looking for a transformation matrix $\mathbf{A}$ such that for a given $\mathbf{W}$ matrix and a set of points $[R_i,r(R_i)]$ the matrices $\bar{\mathbf{W}}[R_i,r(R_i)]; i = 1,N$ are diagonal. These transformation matrices (which are orthogonal) will depend, of course, on the points $[R_i,r(R_i)]$. Thus, if $\mathbf{A}_1$ is chosen so that $\bar{\mathbf{W}}\,[R_1,r(R_1)]$ is diagonal, then Eq. (19) becomes

$$\nabla^2\bar{\psi} + (\bar{\mathbf{W}} - E)\bar{\psi} = 0, \tag{22}$$

where

$$\bar{\mathbf{W}} = \mathbf{A}_1\mathbf{W}\mathbf{A}_1^*$$

and

$$\bar{\psi} = \mathbf{A}_1^*\psi. \tag{23}$$

Having made this transformation, it will be easy to solve Eq. (22) in the vicinity of $R = R_1$. Once this is completed we move to the next point on the adiabatic path, namely $R = R_2$ and repeat this procedure. This is done until the final R value is reached. Thus employing this series of consecutive transformations, Eq. (22) is solved in a representation similar to the adiabatic one, without explicitly introducing the nonadiabatic coupling terms. It should be emphasized that this procedure is "exact" and does not involve any approximations. The equation for $\bar{\psi}$ is more easily solved as the off-diagonal elements of $\bar{\mathbf{W}}(R,r)$ are much smaller in the vicinity of R_1 than those of $\mathbf{W}(R,r)$. Additional details on this procedure are given in Ref. 30.

V. THE INTRODUCTION OF RIOSA

A. Summary of the main equations

Within the RIOSA the differential state-to-state cross section is written in the form[28]

$$\frac{d\sigma^q}{d\Omega}=\frac{1}{8k_{v_i}^2}\sum_{l_i}\sum_{l_i'}(2l_i+1)(2l_i'+1)\times P_{l_i}(\cos\theta)P_{l_i}'(\cos\theta)\times\int_{-1}^{+1}d(\cos\gamma_i)S^q(E_t,\gamma_i,l_i|v_i,v_f)\times S^{q*}(E_t,\gamma_i,l_i'|v_i,v_f) \tag{24}$$

and the state-to-state integral cross section is

$$\sigma^q(E_t|v_i,v_f)=\frac{\pi}{2k_{v_i}^2}\sum_{l_i}(2l_i+1)\times\int_{-1}^{1}d(\cos\gamma_i)|S^q(E_t,\gamma_i,l_i|v_i,v_f)|^2, \tag{25}$$

where E_t is the total energy, v_i and v_f are the initial and final vibrational states ("i" stands for "initial" and "f" for "final"; each refers to a different arrangement channel), k_{v_i} is the initial wave number, l_i is the orbital angular quantum number in the initial channel, γ_i is the IOSA angle as defined in the reagents channel (see Fig. 1) and $S^q(E_t,\gamma_i,l_i|v_i,v_f)$ is an S matrix element where $q=e$ stands for "exchange" and $q=c$ stands for "charge transfer." The calculated S matrix elements also depend on a parameter, the RIOSA B constant, which permits transformation from a given value of γ_i, in the inital arrangement channel to a *single* value of γ_f in the final arrangement channel (see Fig. 1).

In addition to the abovementioned functions we shall also refer to opacity functions $P^q(E_t,l_i|v_i)$ defined as

$$P^q(E_t,l_i|v_i)=\sum_{v_f}\frac{1}{2}\int_{-1}^{+1}d(\cos\gamma_i)|S^q(E_t,\gamma_i,l_i|v_i,v_f)|^2 \tag{26}$$

and to γ-dependent integral cross sections $\sigma^q(E_t,\gamma_i|v_i)$ which hereafter, is called the steric factor:

$$\sigma^q(E_t,\gamma_i|v_i)=\frac{\pi}{k_{v_i}^2}\sum_{v_f}\sum_{l_i}(2l_i+1)|S^q(E_t,\gamma_i,l_i|v_i,v_f)|^2. \tag{27}$$

Keeping γ_i constant means forcing the three-particle system to move on a single plane defined by $\gamma_i=$ const in the three-dimensional coordinate space. Within the RIOSA the three-particle system moves on one plane in the initial arrangement and on the other, defined by $\gamma_f=$ const in the final arrangement. The two planes intersect along a straight line that goes through the origin ($r=R=0$). The parameter B determines the tangent of this line through the relation[27-29]

$$r_f=Br_i, \tag{28}$$

where r_α; $\alpha=i,f$ are the scaled vibrational coordinates of the reagents and the products, respectively. Thus assigning a value to B means fixing the line that separates the reagents channel from the products channel. This line must to follow the ridge of the potential energy surface, since the potential ridge clearly represents the border line between the two arrangement channels.[29] In a symmetric case such as $H+H_2$, the value of B is 1, and this yields the following relation between γ_i and γ_f (see also Fig. 1):

$$\gamma_f=\pi-\gamma_i. \tag{29}$$

In the present case B was found to be different from 1 and consequently the relation between γ_i and γ_f is much more complicated, namely,[27]

$$\cos\gamma_f=-\frac{\cos\gamma_i+(1-B^2)\cot\varphi\cot\beta}{B[1+(1-B^2)\cot^2\varphi]^{1/2}}, \tag{30}$$

where

$$\cot\varphi=\frac{\sin\beta}{B^2-\cos^2\beta}[\cos\beta\cos\gamma_i+(B^2-\sin^2\gamma_i\cos^2\beta)^{1/2}] \tag{31}$$

and

$$\cos\beta=-\frac{m_A m_C}{(m_A+m_B)(m_C+m_B)}. \tag{32}$$

Here, m_B and m_C are the masses of the two hydrogen atoms and m_A is the mass of argon. The angle β is the skewing angle, a characteristic angle for the three-particle reactive system.

To calculate the S matrix elements, one solves the collinear-type coupled Schrödinger equations:

$$\left[-\frac{\hbar^2}{2\mu}\left(\frac{\partial^2}{\partial R_\alpha^2}+\frac{\partial^2}{\partial r_\alpha^2}\right)+W_{11}+\frac{\hbar^2 l_\alpha(l_\alpha+1)}{2\mu R_\alpha^2}-E\right]\psi_1(R_\alpha,r_\alpha;\gamma_\alpha)+W_{12}\psi_2(R_\alpha,r_\alpha;\gamma_\alpha)=0,$$
$$\left[-\frac{\hbar^2}{2\mu}\left(\frac{\partial^2}{\partial R_\alpha^2}+\frac{\partial^2}{\partial r_\alpha^2}\right)+W_{22}+\frac{\hbar^2 l_\alpha(l_\alpha+1)}{2\mu R_\alpha^2}-E\right]\psi_2(R_\alpha,r_\alpha;\gamma_\alpha)+W_{12}\psi_1(R_\alpha,r_\alpha;\gamma_\alpha)=0. \tag{33}$$

Here $\alpha=i,f$ and $\gamma_\alpha;\alpha=i,f$ enter as parameters, r_α and R_α are the mass-scaled vibrational and translational coordinates, and μ is the reduced mass of the system, i.e.,

$$\mu=\left(\frac{m_A m_B m_C}{m_A+m_B+m_C}\right)^{1/2}. \tag{34}$$

W_{11} and W_{22} are the two diagonal elements of the potential matrix, or, in other words, the diabatic surfaces; W_{12}, the off-diagonal term, is the diabatic coupling term [see Eqs. (6)] and l_α; $\alpha=i,f$ are the orbital angular quantum numbers. Since the calculations are carried out for each given l_i,l_f is defined as the closest integer to the solution of the equation

$$l_f(l_f+1)=C(\gamma_i,B)l_i(l_i+1), \tag{35}$$

where $C(\gamma_i,B)$ is a known explicit function of γ_i and B.[29] For a symmetric case $C(\gamma_i,B)$ is equal to 1 and consequently $l_f=l_i$.

As can be noticed, Eqs. (33) can be solved for a given set of values of γ_i,l_f and B. However, whereas l_i and γ_i are variables, B is a constant (or, eventually, a series of constants) yet to be determined. A detailed description of how this is done is given in Ref. 29. We shall briefly describe it here too, mainly in order to introduce the relevant facts regarding the $(Ar+H_2)^+$ system.

B. Derivation of the matching parameter B

The parameter B determines the position of the dividing line along which the reagents and the products wave functions have to be matched in order to obtain a continuous wave function for each γ_i and l_i. The physical aspect of this line is that for a given γ_i, it divides the whole configuration space into two regions, one corresponding to the reagents arrangement and the other to the products arrangement. In order to be more specific, we shall refer to the collinear case $(\gamma_i=0;\gamma_f=\pi)$. Here the line is expected to follow the position of the potential ridge. The position of the ridge is best obtained by employing the hyperspherical coordinates ρ and η and drawing the potential as a function of η for different values of ρ. Such curves for the (lowest) abiabatic surface (which is the only reactive surface) of the $(Ar+H_2)^+$ system are shown in Fig. 7(a). Each curve consists of two wells corresponding to the positions of the two arrangement channels and a barrier between them. Three curves are shown for three different values of ρ, i.e., $\rho=7,8,9$ a.u. The ridge line is defined as the line passing through all the maximum points. As can be seen, this line is almost straight and perpendicular to the η axis. Thus it is characterized by one η value, i.e., $\eta=\eta_m$. This value describes in the (R,r) plane a line that passes through the origin $(r=0,R=0)$. In a similar way one can find such a line for each γ_i. In Fig. 7(b) we show a line like that for $\gamma_i=\pi/2$. Determining the position of the line yields the value of B. It was found that for $\gamma_i=0$ the value of B is 1.5 and for $\gamma_i=\pi/2$ the value is 1.4. Thus B is close to being constant.

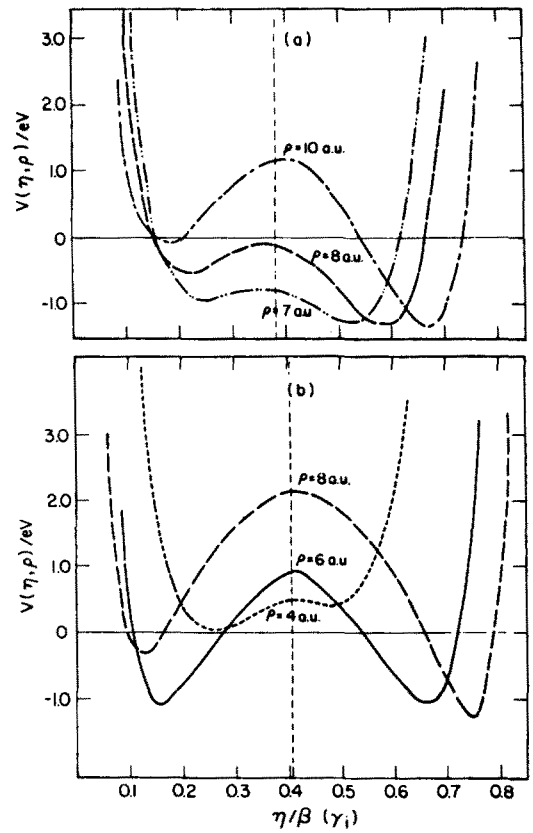

FIG. 7. The double minimum potential energy curves at fixed values of the hyperradius ρ as a function of the hyperangle η for the lowest adiabatic $(A_r+H_2)^+$ system. η is given in units of β, the corresponding skewing angle. (a) The collinear case; $\beta(\gamma_i=0)=45.7°(0.798$ rad). The corresponding value of B is 1.5. (b) The $\gamma_i=90$ case; $\beta(\gamma_i=90°)=75.9°$ (1.324 rad). The corresponding value of B is 1.4.

VI. NUMERICAL DETAILS

The calculations were performed for one total energy value $E_{tot}=0.6$ eV. At this energy the following asymptotic states are open (see Fig. 8):

$$Ar^+ + H_2: v_i=0;\ E_v=0.444\ \text{eV};\ E_{t_i}=0.156\ \text{eV},$$

$$Ar + H_2^+: v_i=0,1;\ E_{v_i}=0.146, 0.424\ \text{eV};$$

$$E_{t_i}=0.454, 0.176\ \text{eV},$$

$$ArH^+ + H: v_i=0\text{–}6;$$

$$E_{v_i}=-1.169,-0.867,-0.578,-0.302,-0.040,$$

$$+0.209, 0.443\ \text{eV},$$

where the E_v's are the vibrational energies and the E_t's are the corresponding translational energies. To obtain $S(E_t,l_i,\gamma_i|v_i,v_f)$ the range $(0,\pi/2)$ of γ_i was divided by ten

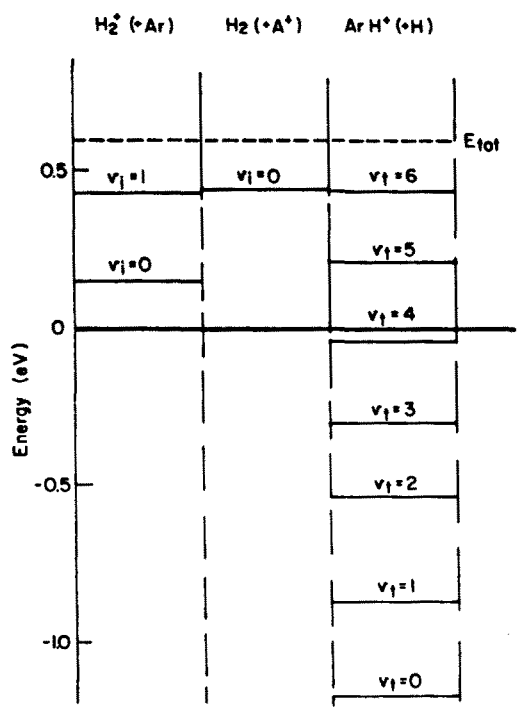

FIG. 8. The (relative) eigenvalues of $H_2^+(+A_2)$, $H_2(+A_2^+)$ and $ArH^+(+H)$. The dotted line stands for $E_{tot}=0.6$ eV.

grid points, such that $\Delta\gamma_j = \gamma_j - \gamma_{j-1} = 10°$. At each given grid point, the coupled system of Schrödinger equations was solved for each value of l_i. The number of necessary l_i's varied from one value of γ_i to the other. The largest number was 87 (for $\gamma_i = 0$ the collinear arrangement) and the smallest was 67 (for $\gamma_i = \pi/2$). Thus altogether the coupled system of Schrödinger equations was solved ~ 750 times.

In order to obtain reliable results we had to include closed vibrational channels. The number of these was increased until convergence was obtained. The rate of convergence depended mainly on l_i. Thus whereas for small values of l_i around 45 states were needed (30 from the lower surface and 15 from the upper one), only around 30 (20:10) states were needed when l_i became 50 or larger.

To obtain differential cross sections we employed Eq. (24). However, since the final curves were rather oscillatory the following smoothing process was employed:

$$\left.\frac{d\bar{\sigma}}{d\Omega}\right|_{\theta=\bar{\theta}} = A\int_{-\pi}^{\pi} d\theta\, e^{-\alpha(\theta-\bar{\theta})^2}\frac{d\sigma}{d\Omega}, \tag{36}$$

where $\alpha^{-1} = 4°$ ($d\sigma/d\Omega$ was calculated for $\Delta\theta = 1°$) and A is a normalization factor.

Since in what follows we refer only to l_i and γ_i (l_f and γ_f are no longer mentioned) we shall delete the index "i."

VII. RESULTS AND DISCUSSION

A. The steric factor

The steric factor is defined as γ-dependent cross sections, introduced in Eq. (27). The results of the calculations for all six processes are shown in Fig. 9; the results for exchange are given in Fig. 9(a) and those for charge transfer in Fig. 9(b). The γ dependences for the two processes are significantly different; whereas the curves for charge transfer are only weakly dependent on γ, a strong dependence is obtained for the exchange process. The results for the exchange are somewhat unexpected because the potential employed here is only weakly dependent on γ and, therefore, the strong dependence should be attributed to the kinematics of the exchange.

To gain more insight we once again employ the hyperspherical coordinates with respect to the lower surface (the surface on which the reaction process takes place). This is done by calculating eigenvalues with respect to the angle η for different ρ values. These eigenvalues and potential ridge are presented as a function of ρ in Fig. 10. We show results for three different γ values, namely, $\gamma = 0°, 60°, 90°$. In general, one distinguishes between two kinds of curves, those related to the reagents and those to the products. The two kinds cross each other, but whether they interact (nonadiabatically) or not depends on how far the (avoided) crossing points are from the position of the ridge line. It is noticed that the larger is γ the deeper is the position of the ridge in the interaction region. In the γ-dependent exchange cross sections two minima were encountered, one around $\gamma = 30°$ and the other for $\gamma = 90°$. Whereas the reason for the decrease around $\gamma = 30°$ is not clear, Fig. 10(c) yields a very nice explanation why the values of $\sigma(\gamma)$ are smallest near $\gamma = 90°$. It can be easily noticed that the ridge is located at a position where the reagents and the products curves no longer cross but are located parallel to each other. Such a situation is well known to be very ineffective for causing nonadiabatic transitions. Consequently, the exchange process is very unfavorable. In the two other cases, the position of the ridge is located in the vicinity of crossing points and consequently nonadiabatic transitions are expected.

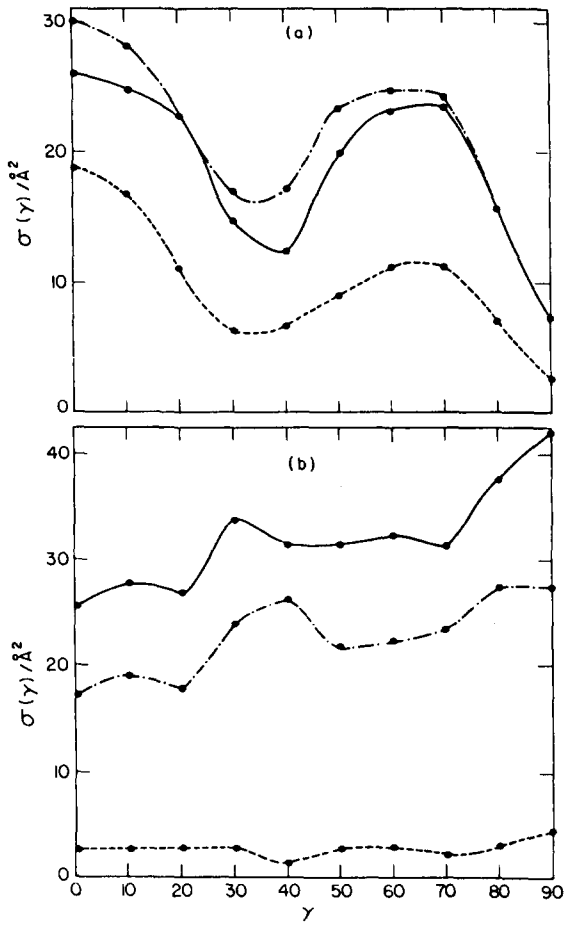

FIG. 9. γ-dependent cross sections for all six reactions (IIa)–(IIf). (a) Cross sections for exchange; (b) cross sections for charge transfer. — $Ar^+ + H_2(v_i = 0)$; --- $Ar + H_2^+(v_i = 0)$; -·-·- $Ar + H_2^+(v_i = 1)$.

The fact that the steric effect for charge transfer is small indicates an isotropic charge distribution in the system. However, this is expected because the potential energy surface is close to being isotropic. Still, the kinematic effects encountered for the exchange process around $\gamma = 90°$ affect the charge transfer process, because those reagents which, upon *approaching* each other, neither react nor exchange charge get another "chance" to exchange charge upon *receding*. Thus for a given γ the smaller the cross section for reaction, the larger is the charge transfer probability for the receding reagents and consequently the larger is the overall cross section for charge transfer.

B. The opacity function

Opacity functions are l-dependent transition probabilities, as introduced by Eq. (26). The results for all six processes are presented in Fig. 11. The main features to be noticed are as follows:

(1) The opacity functions for exchange are relatively

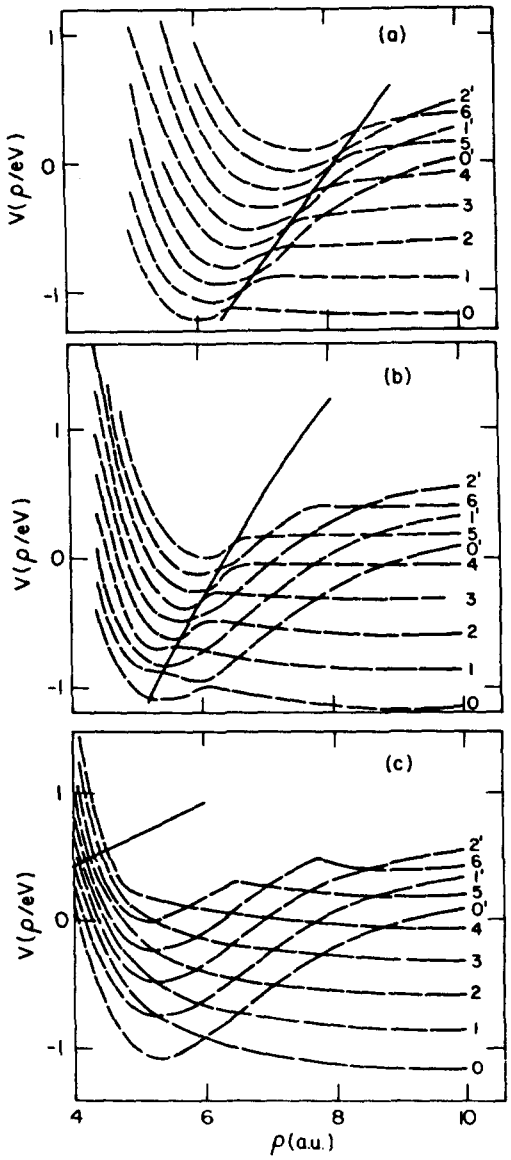

FIG. 10. Adiabatic potential (eigen) energies as a function of the hyperradius ρ for the lowest adiabatic surface, for different γ values. (a) The collinear case—$\gamma_i = 0$; (b) $\gamma_i = 60°$; (c) $\gamma_i = 90°$. The full line is the ridge line.

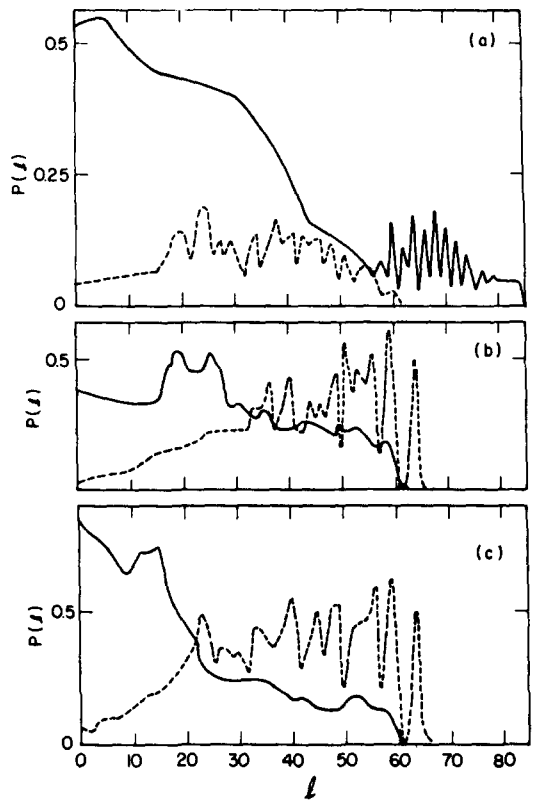

FIG. 11. Opacity probabilities as a function of the orbital angular quantum number l_i: (a) Results for $Ar + H_2^+ (v_i = 0)$; $E_{tr} = 0.454$ eV. (b) Results for $Ar + H_2^+ (v_i = 1)$; $E_{tr} = 0.154$ eV. (c) Results for $Ar^+ + H_2 (v_i = 0)$; $E_{tr} = 0.156$ eV. — Exchange; --- charge transfer.

smooth and, in general, a decreasing function with respect to l.

(2) The opacity functions for charge transfer are at first smooth and an increasing function of l. Later they reach a plateau region and become oscillatory. The oscillations obtained in all three cases of charge transfer processes are reminiscent of what is encountered in charge transfer studies of ion–atom collisions and is considered to be a result of interference effects. It is gratifying to find out that this feature exists also within an approximation where the final opacity functions are obtained from an integration of probabilities over the angle γ.

(3) The opacity functions for reagents $Ar + H_2^+ (v_i = 1)$ and $Ar^+ + H_2$ are similar in many details, in particular those for charge transfer, indicating that the two reagents are almost in resonance.

(4) The opacity function for reagents $Ar + H_2^+ (v_i = 0)$ differs from the others in two ways [see Figs. 11(a) and 11(b)].

(a) The opacity function for reaction (IIa) extends to higher l values, although while doing so the function becomes oscillatory. This extension is due to the larger translational energy available for reactions (IIa) and (IIb).

(b) The opacity function for reaction (IIb) is much smaller because in this case the charge transfer process must be accompanied by a significant change of linear momentum, a process rather unlikely in such cases.

(5) The exchange process (IIa) [Fig. 11(a)] extends to larger l values than the corresponding charge transfer process (IIb); the reason is that the S matrix is Hermitian (and consequently the probability matrix is symmetric) which means that if for a given l, process (IIb) takes place then the reverse process (IIf) also must take place and vice versa. However, since process (IIf) is inhibited for large l values due to the low translational energy available in this case, the same is expected for reaction (IIf). As for the exchange process (IIa), such limitations are not encountered.

In Fig. 12 the RIOSA opacity functions are compared with those obtained for a TSH calculation. The comparison is carried out for reactions (IIe) and (IIf). Whereas the results may look similar to a certain extent (large exchange probabilities in the low l region vs large charge transfer probability in the high l region), they differ in many details. It is noticed that the RIOSA exchange probabilities are much

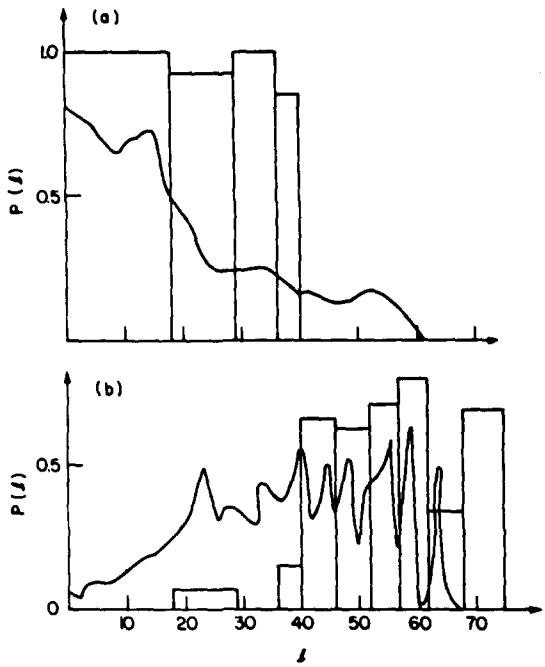

FIG. 12. Comparison between RIOSA (curves) and TSH (histograms) opacity functions for $Ar^+ + H_2(v_i = 0)$. (a) Exchange; (b) charge transfer. (The RIOSA results are for $E_t = 0.156$ eV and the TSH for $E_t = 0.130$ eV.)

smaller than the TSH probabilities, but they extend to larger l values. A better agreement is obtained for the charge transfer probabilities [Fig. 12(b)] but nevertheless the quantum curve extends to much smaller l values and the TSH to larger ones.

C. Differential cross sections

The differential cross sections were calculated employing Eq. (24). However, since the final curves were rather oscillatory, a smoothing process was introduced [cf. Eq. (36)]. The results for all six processes are shown in Fig. 13. Each box shows two curves, one for the exchange and the other for charge transfer. The main features to be noticed:

(1) All six curves extend from zero to π. Each curve is characterized by two maxima, one in the forward direction, i.e., near $\theta = 0$, and the other in the backward direction, i.e., near $\theta = \pi$. The forward peak is much broader, emphasizing the contributions of the large impact parameters.

(2) The two systems in near resonance, namely $Ar^+ + H_2$ and $Ar + H_2^+ (v_i = 1)$ have very similar angular dependence. In particular, in case of charge transfer they are both characterized by one additional pronounced maximum around $\theta = 50°$.

(3) It is not always clear how to relate the particular shape of the opacity function given in Fig. 11 with the angular distributions shown in Fig. 13. For instance, it is clear why the angular distribution for charge transfer in case of $Ar^+ + H_2$ and the exchange process in case of $Ar + H_2^+ (v_i = 0)$ show a higher forward peak than the corresponding peaks of the competitive reactions (higher probabilities in the large l region). However, it is not clear why in the case of $Ar + H_2^+ (v_i = 1)$ the charge transfer forward

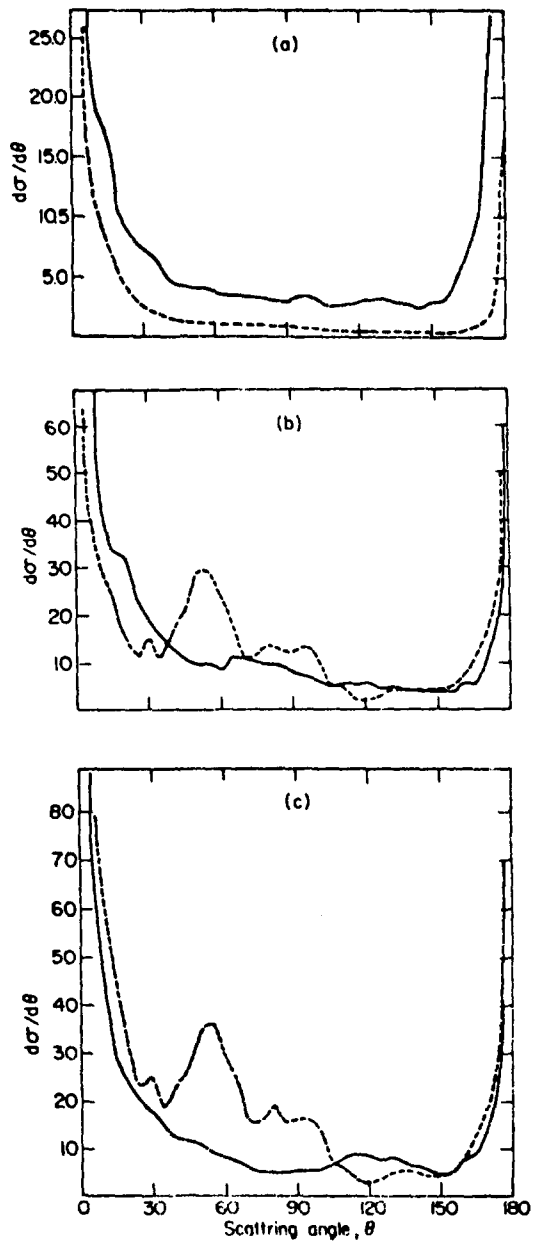

FIG. 13. Differential cross sections (a) for $Ar + H_2^+ (v_i = 0)$; (b) for $Ar + H_2^+ (v_i = 1)$; (c) for $Ar^+ + H_2(v_i = 0)$. — Exchange; --- charge transfer.

peak is not higher than the one for exchange, in spite of the higher charge transfer probabilities in the large l region. The source for this discrepancy is related to the fact that the calculation of *differential* cross sections is based on S matrix elements and not on probabilities [see Eq. (24)].

Although several experimental studies yield an angular distribution of products, a direct comparison could be made in one case only, namely, for the charge transfer in $Ar^+ + H_2$. Hierl *et al.*[16] measured the angular distributions for this system for different energies. The comparison between the quantum mechanical and the experimental results for $E_t = 0.13$ eV (a value close to our 0.156 eV) is shown in Fig. 14. The fit between the two distributions is reasonable. In particular, it is gratifying to see that both the

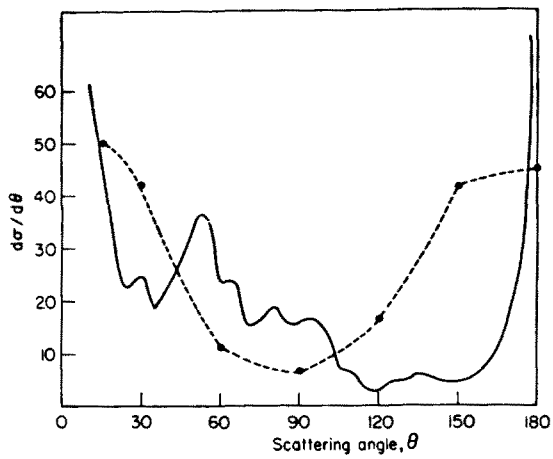

FIG. 14. Comparison between experimental and RIOSA differential cross sections for $Ar^+ + H_2(v_i = 0) \rightarrow Ar + H_2^+$. --- Experimental; — RIOSA.

forward and the backward experimental peaks are reproduced by the quantum treatment.

We want to call attention to another feature found in both the experimental and theoretical treatments. From Figs. 13(b) and 13(c), it is well noticed that the angular distributions for the two (near resonance) charge transfer processes, namely, $Ar^+ + H_2$ and $Ar + H_2^+ (v_i = 1)$, are almost identical. Such a close relation was also found in experiment when we compare the results of Hierl *et al.*[16] for $E_t = 0.48$ and the results of Bilotta *et al.*[18] for $E_t = 0.45$ eV (Bilotta *et al.*[18] studied the reverse reaction, but with a Franck–Condon vibrational distribution for the H_2^+ molecule). The angular distributions in the two studies are very similar.

Although Bilotta *et al.*[17] reported on differential cross sections for exchange, no direct comparison can be carried out because either their initial translational energy is too high [and in this case our $Ar + H_2^+ (v_i = 1)$ results are not relevant] or their (initial) vibrational state distribution H_2^+ is different (the Franck–Condon distribution, is far from being a dominant ground state).

The comparison with the TSH results[25] does not yield a clear picture mainly because at each energy the TSH results come from a sampling of only 200–300 trajectories in case of $Ar^+ + H_2$ and 100–200 in case of $Ar + H_2^+$. The TSH study yields an isotropic distribution for the exchange process, whereas products are missing at the two extremes of the angular range (i.e., $\theta \sim 0; \theta \sim \pi$). On the other hand, our results show prominent peaks at the two ends of the angular range. As for charge transfer, the TSH yields only the forward peak and is in contradiction with both, the experimental and the quantum results.

D. Integral cross section

Results are shown in Tables I and II. In Table I the RIOSA results are compared with (quantum) "collinear"-type results, as obtained from Eq. (27) by substituting $\gamma_i = 0$ and with the TSH results.[25] In Table II the RIOSA results are compared with experimental results, namely, those of Tanaka *et al.*,[8,9] Houle *et al.*,[15] and Ervin and Armentrout.[12]

1. Comparison with other theoretical calculations

From Table I it is well noticed that, in general, the TSH cross sections are larger than the quantum ones, but except for the cross section of reaction (IIa) the ratio between the results obtained by the different methods never exceeds 2:1. In general, the discrepancy is larger for the exchange. For charge transfer we have a remarkable fit for processes (IIb) and (IId) but a relatively large discrepancy for reaction (IIf). However, this last result within the TSH method seems to be a manifestation of the inadequacy of the TSH method for correct treatment of charge transfer processes, at least in the low energy region.[31] The reason is that microscopic reversibility is not necessarily fulfilled within classical mechanics (it was shown several times in the past that this failure causes difficulties with classical results.[32] In order to see the contradiction due to this failure, we analyze the present case. For $E_{tot} = 0.6$ eV, we have one open state for $Ar^+ + H_2$ and two for $Ar + H_2^+$ (see Sec. VI and Fig. 8). Fulfillment of the microscopic reversibility roughly requires the following relation to hold:

TABLE I. Comparison of theoretical cross sections for exchange and charge transfer processes as obtained within different frameworks (numbers in $Å^2$).

Reagents	Trans.[a] energy (eV)	Products	RIOSA (3D)	Collinear	TSH[c]
$Ar + H_2^+ (v_i = 0)$	0.454	$ArH^+ + H$	8.8	18.8	31.0
	(0.440)	$Ar^+ + H_2$	2.6	2.4	0.8
$Ar + H_2^+ (v_i = 1)$	0.176	$ArH^+ + H$	20.0	30.3	37.0
	(0.180)	$Ar^+ + H_2$	24.0	17.2	31.0
$Ar^+ + H_2(v_i = 0)$	0.156	$ArH^+ + H$	6.1[b]	8.7[b]	13.0[b]
	(0.130)	$Ar + H_2^+$	11.1[b]	8.5[b]	23.3[b]

[a] These numbers were used in the RIOSA calculations; the ones in parentheses are those used in the TSH study.
[b] The original numbers were divided by 3 for statistical reasons.
[c] Results from Ref. 25.

TABLE II. Comparison between experimental and RIOSA cross sections (numbers in Å^2).

Reagents	Trans.[a] energy (eV)	Products	RIOSA	Tanaka *et al.*[b]	Houle *et al.*[c]	Ervin and Armentrout[d]
$Ar + H_2^+(v_i=0)$	0.454	$ArH^+ + H$	8.8	28	70	···
		$Ar^+ + H_2$	2.6	~0	2.5	···
$Ar + H_2^+(v_i=1)$	0.176	$ArH^+ + H$	20.0	33	80	···
		$Ar^+ + H_2$	24.0	3	18	···
$Ar^+ + H_2(v_i=0)$	0.156	$ArH^+ + H$	6.1	70	···	30
		$Ar^+ + H_2$	11.1	3	···	2

[a] Values used in the RIOSA treatment.
[b] References 8 and 9.
[c] Reference 15.
[d] Reference 12.

$$P_c[Ar^+ + H_2(v_i=0)] = P_c[Ar + H_2^+(v_i=0)] + P_c[Ar + H_2^+(v_i=1)]. \quad (37)$$

Here $P_c(I)$s are the probabilities defined as

$$P_c(I) = E_t\sigma^c(I), \quad (38)$$

where $\sigma^c(I)$ is the charge transfer cross section for the initial channel I. Equations (37) and (38) yield

$$\sigma^c[Ar^+ + H_2(v_i=0)] = \frac{0.44}{0.13}\sigma^c[Ar + H_2^+(v_i=0)] + \frac{0.18}{0.13}\sigma^c[Ar + H_2^+(v_i=1)]. \quad (39)$$

Inserting the respective TSH cross sections for charge transfer yields $\sigma^c[Ar^+ + H_2(v_i=0)] = 45.9$ Å^2. In the actual calculations the value of $(3\times 23.3) = 69.9$ Å^2 was obtained. The discrepancy between the two values i.e., 45.9 and 69.9 Å^2, seems to be somewhat large. The TSH value as obtained from Eq. (39), i.e., $0.33\times 45.9 = 15.3$ Å^2 fits reasonably well with the RIOSA value, i.e., 11.1 Å^2.

On the other hand, the microscopic reversibility requirement holds very nicely for the quantum mechanical results. The calculated value for $Ar^+ + H_2(v_i=0) \rightarrow Ar + H_2^+(v_i=0,1)$ is $(3\times 11.1) = 33.3$ Å^2 as compared to 34.6 Å^2 obtained from the right-hand side of Eq. (39).

In Table I are also presented collinear-type results and it is noticed that whereas the TSH cross sections fit better the RIOSA results for charge transfer, they fit better the collinear ones for exchange.

2. Comparison with experimental results

The discrepancy between the RIOSA and the experimental results as presented in Table II is, to a certain extent, disappointing. There could be several reasons for that, but at least one of them is the inaccuracy of the potential energy surfaces. The potential was furnished in 1972 and since then no efforts were made to modify it to improve the fit between theory and experiment. Moreover, it is important to remember that the potential is semiempirical and not supported by any *ab initio* study. One of the main inaccuracies is connected with the relative positions of the asymptotic vibrational states of $Ar + H_2^+(v_i=0,1,2)$ and $Ar^+(^2P_{3/2},^2P_{1/2}) + H_2(v_i=0)$. Since the calculations are done with only two surfaces, we had to form one weighted state out of the two spin states of Ar^+, a fact which shifted the ground vibrational eigenstate of H_2 to a wrong position with respect to those of $Ar + H_2^+(v_i)$. This fact can have an appreciable influence on the cross sections for both the exchange and charge transfer.

Except for the occasional incompatibility between theory and experiment Table II also shows a large discrepancy among the experimental results measured in the different laboratories, and so it is not always clear to which of the experimental results one should compare the theoretical ones. For instance, we find a very good fit between theory and experiment for reaction (IIb) (all three treatments yield relatively small cross sections) but as for the cross section for reaction (IId): On the one hand, it fits very nicely the result of Houle *et al.*[15] but it is much too large when compared to the results of Tanaka *et al.*[9] As for the exchange, it is noticed that the quantum result for reaction (IIa) is much smaller than both experimental results (although again, there are large differences between the two) but as for reaction (IIc), it is much smaller than Houle *et al.*'s[15] result but in a reasonable fit with Tanaka *et al.*'s[9] value.

The results for the reagents $Ar^+ + H_2$ seem to be even more disappointing. The exchange cross section is much too small and the charge transfer cross section too large. However, here we would like to point out again a possible internal inconsistency with results of Tanaka *et al.*[8] The latter authors measured charge transfer cross sections as a function of energy for several cases, including the three reactions [(IIb), (IId), and (IIf)] mentioned here. They found that the results hardly depend on energy, and consequently we shall concentrate on their results for $E_t = 0.48$ eV. In addition to the two values listed in Table II, namely, $\sigma^c \sim 0.0$, 3.0 Å^2, we also refer to their third value, namely $\sigma^c(v_i=2) \sim 25$ Å^2. The microscopic reversibility rule, as described above, implies that {recalling $\sigma^c[Ar + H_2^+(v_i=0)] = 0$}:

$$\sigma^c[Ar^+ + H_2(v_i=0)] = \frac{0.55}{0.30}\sigma^c[Ar + H_2^+ + (v_i=1)] + \sigma^c[Ar + H_2^+(v_i=2)]. \quad (40)$$

(The translational energy values were taken from Refs. 8 and 9.) Substituting the corresponding values for the two σ^c values yields $\sigma^c[Ar^+ + H_2(v_i=0)] = 30.5$ Å^2. This result must be divided by three (for statistical reasons), namely, $\sigma^c[Ar^+ + H_2(v_i=0)] = 10.2$ Å^2 in contrast to the directly measured value of 3–5 Å^2 (Ref. 8) (it is interesting that the RIOSA result is in good fit with this value). This inconsistency might be due to the possible large error bars in the case of $Ar^+ + H_2$. Still, we think that more experimental work is needed to resolve the large differences between the experimental results.

3. Final vibrational distribution for exchange

Final vibrational distributions are given in Fig. 15. This figure gives two kinds of results, the present RIOSA results and the collinear-type results obtained from Eq. (27) by taking the $\gamma = 0$ case. All results are normalized to 1 at their highest value. It is noticed that whereas in the collinear case the population inversion is obtained in all three cases [although for $Ar + H_2^+$ $(v_i = 0)$ the inversion is only with respect to $v_i = 1$], no inversion was encountered in the full 3D case; all three curves are monotonically decreasing functions of v_f.

In Table III we show average values for final translational energy $\overline{E}_{t_f}$, and final vibrational energy $\overline{E}_{v_f}$, and final vibrational quantum numbers $\overline{v}_f$. Again two quantum results are shown, the regular (RIOSA) three-dimensional ones and the collinear ones [Eq. (27)].

These and the previous results can be compared with the TSH cross sections. The comparison shows that the TSH products are somewhat more (vibrationally) excited than the RIOSA products (on the average, the shift is, by one vibrational state). As for the collinear quantum results they seem to be fit rather nicely, the TSH ones. However, it should be mentioned that the TSH results for $Ar + H_2^+$ $(v_i = 0,1)$ were calculated for much higher energies.

VIII. SUMMARY

The main conclusions obtained in this study are:

(a) The RIOSA integral cross sections are in qualitative agreement with both the TSH and the experimental ones. The discrepancy with the TSH results is usually in the range of 1:1 to 1:2, whereas the range with the experimental ones is 1:1 to 1:6. The source for the relatively large discrepancy with the experimental results is at least partly an inadequacy of the potential surfaces employed. However, it should be mentioned that experimental results obtained in different laboratories sometimes deviate significantly and there may be some internal inconsistencies among the results due to unfulfillment of the microscopic reversibility.

(b) As a general statement we may say that the agreement of the present results with the quasiclassical results, and with the experimental results is much better for charge transfer than for the exchange process.

(c) One of the gratifying results obtained in this study is the nice fit between the experimental and the quantum differential cross sections for the charge transfer process $Ar^+ + H_2(v_i = 0) \rightarrow Ar + H_2^+$. The significance of this finding is enhanced by the fact that the TSH treatment yields angular distributions which are far removed from the experimental ones.

(d) Opacity functions were calculated and compared with the TSH functions. There were some general similarities but they were found to differ in many significant details. In particular, we found that for the reaction $Ar^+ + H_2 \rightarrow Ar + H_2^+$ the TSH opacities differ from zero for large impact parameters only, whereas the quantum ones extend to much lower values. This fact explains, for instance, why the backwards tail in the TSH differential cross section is missing and why it exists in the quantum results (in accordance with experiment).

(e) One of the advantages of employing the IOSA is that it yields in a direct manner the steric effect for the reaction under consideration. The present study, like the one for $He + H_2^+$ [29,33] revealed a surprising result in this respect. It was found that although the potentials employed are only weakly dependent on the angle of approach γ, and the γ-dependent cross sections for *exchange* were strongly dependent on that angle; they were oscillatory (one oscillation for

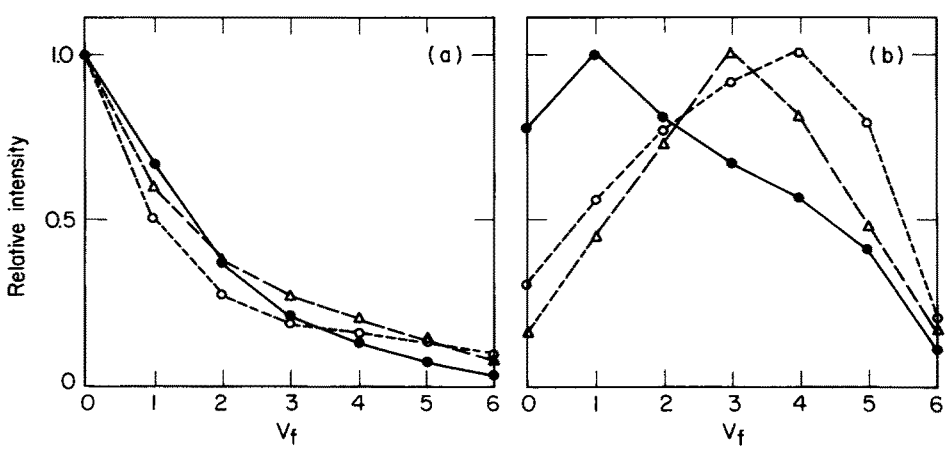

FIG. 15. Quantum final vibrational-state distribution for exchange. (a) Three-dimensional (RIOSA) results; (b) collinear results [Eq. (27) for $\gamma_i = 0$]. ● $Ar + H_2^+$ $(v_i = 0)$; ○ $Ar + H_2^+$ $(v_i = 1)$; △ $Ar^+ + H_2(v_i = 0)$.

TABLE III. Final average translational and vibrational energies and final average vibrational quantum numbers as obtained in the quantum mechanical treatment.

Reagent	Trans. energy (eV)	Three-dimensional (RIOSA)			One-dimensional		
		$\overline{E}_{t_f}$(eV)	$\overline{E}_{v_f}$(eV)	$\overline{v}_f$	$\overline{E}_{t_f}$(eV)	$\overline{E}_{v_f}$(eV)	$\overline{v}_f$
$Ar + H_2^+ (v_i = 0)$	0.454	1.39	0.51	1.2	1.11	0.79	2.2
$Ar + H_2^+ (v_i = 1)$	0.176	1.32	0.58	1.4	0.87	1.03	3.1
$Ar^+ + H_2 (v_i = 0)$	0.156	1.30	0.60	1.5	0.88	1.02	3.0

the $0 < \gamma < \pi$ interval) and had a tendency to reach the minimum at $\gamma = \pi$. In case of charge transfer these cross sections were only weakly dependent on γ, as one would expect. This strong dependence for exchange hints on the existence of a hidden steric factor, associated not with the potential, but rather with the kinematics of the exchange process itself. More research is needed to understand this behavior.

(f) As a final point we shall briefly refer to the relevance of the RIOSA for such a system. The IOSA becomes more relevant when at least one of the two following conditions is met: (1) For a mass combination such that the atom is light and the diatomic heavy ($H + D_2$ might be a good example). In such a case γ is unlikely to vary, at least for $1 \sim 0$; (2) for a potential which is only weakly dependent on γ (a breathing sphere-type potential). In the extreme case, the IOSA becomes exact. In our study the second condition is met, and therefore we expect our results to be relevant (assuming the potential to be correct).

ACKNOWLEDGMENTS

One of us (M. B.) would like to thank Professor Sally Chapman for making available her $(ArH_2)^+$ DIMZO program and for valuable telephone conversations and correspondence regarding the details of the potential energy surfaces. Also, he would like to thank her for sending him a few additional TSH cross sections which were not published. This work was supported in part by a Grant-in-Aid from the Ministry of Education, Science, and Culture of Japan. Numerical calculations were carried out at the computer center of the Institute for Molecular Science.

[1]P. M. Langevin, Ann. Chem. Phys. **5**, 245 (1905).
[2](a) T. Su and M. T. Bowers, J. Chem. Phys. **58**, 3027 (1978); (b) M. Quack and J. Troe, Ber. Bunsenges. Phys. Chem. **78**, 240 (1978); **79**, 170, 469 (1975); (c) J. Troe, Chem. Phys. Lett. **122**, 425 (1985).
[3]W. J. Chesnavich and M. T. Bowers, Progr. React. Kinet. **11**, 137 (1982).
[4]D. C. Clary, Mol. Phys. **54**, 605 (1985); D. C. Clary, D. Smith, and N. G. Adams, Chem. Phys. Lett. **119**, 320 (1985).
[5]A. Henglein, K. Lacmann, and G. Jacobs, Ber. Bunsenges. Phys. Chem. **64**, 279 (1965).
[6]P. M. Hierl, Z. Hermann, and R. Wolfgang, J. Chem. Phys. **53**, 660 (1970).
[7]T. Turner, O. Dutuit, and Y. T. Lee, J. Chem. Phys. **81**, 3475 (1984).
[8]K. Tanaka, J. Durup, T. Kato, and I. Koyano, J. Chem. Phys. **74**, 5561 (1981).
[9]K. Tanaka, T. Kato, and I. Koyano, J. Chem. Phys. **75**, 4941 (1981).
[10]K. Lacmann and A. Henglein, Ber. Bunsenges. Phys. Chem. **69**, 286 (1965).
[11]R. C. Amme and J. F. McIlwain, J. Chem. Phys. **45**, 1224 (1966).
[12]K. M. Ervin and P. B. Armentrout, J. Chem. Phys. **83**, 166 (1985).
[13]W. A. Chupka and M. E. Russell, J. Chem. Phys. **49**, 5426 (1968).
[14]F. M. Campbell, R. Browning, and C. J. Latimer, J. Phys. B **13**, 4257 (1980).
[15]F. A. Houle, S. L. Anderson, D. Gerlich, T. Turner, and Y. T. Lee, J. Chem. Phys. **77**, 748 (1982).
[16]P. M. Hierl, V. Pacak, and Z. Herman, J. Chem. Phys. **67**, 2678 (1977).
[17]M. Bilotta, F. N. Prehminger, and J. M. Farrar, J. Chem. Phys. **73**, 1637 (1980).
[18]M. Bilotta, F. N. Prehminger, and J. M. Farrar, Chem. Phys. Lett. **74**, 95 (1980).
[19]P. J. Kuntz and A. C. Roach, J. Chem. Soc. Faraday Trans. 2 **68**, 259 (1972).
[20]S. Chapman and R. K. Preston, J. Chem. Phys. **60**, 650 (1974).
[21]M. Baer and J. A. Beswick, Chem. Phys. Lett. **51**, 360 (1977); Phys. Rev. A **19**, 1559 (1979).
[22]M. Baer, Mol. Phys. **35**, 1637 (1978).
[23]Z. H. Top and M. Baer, Chem. Phys. **25**, 1 (1977); J. Chem. Phys. **66**, 1363 (1977).
[24]J. M. Yuan and D. Micha, J. Chem. Phys. **64**, 1032 (1975).
[25]S. Chapman, J. Chem. Phys. **82**, 4033 (1985). A few of the lower energy cross sections were obtained through private communication.
[26]M. Baer, Adv. Chem. Phys. **49**, 191 (1982); J. Jellinek and D. J. Kouri, in *Theory of Chemical Reaction Dynamics*, edited by M. Baer (Chemical Rubber, Boca Raton, 1985), Vol. II, Chap. 1; D. C. Clary and J. P. Henshaw, in *The Theory of Chemical Reaction Dynamics*, edited by D. C. Clary (Reidel, Dordrecht, 1986).
[27]V. Khare, D. J. Kouri, and M. Baer, J. Chem. Phys. **71**, 1188 (1979); M. Baer, D. J. Kouri, and J. Jellinik, *ibid.* **80**, 1431 (1984).
[28]J. M. Bowman and K. T. Lee, J. Chem. Phys. **72**, 5071 (1980).
[29]H. Nakamura, A. Ohsaki, and M. Baer, J. Phys. Chem. **90**, 6176 (1986).
[30]In *Theory of Chemical Reaction Dynamics*, edited by M. Baer (Chemical Rubber, Boca Raton, 1985), Vol. 2, Chap. 4.
[31]M. Baer, H. Nakamura, and A. Ohsaki, Chem. Phys. Lett. **131**, 468 (1986).
[32]H. Essen, G. D. Billing, and M. Baer, Chem. Phys. **17**, 443 (1976); S. Ron, E. Pollak, and M. Baer, J. Chem. Phys. **78**, 4414 (1983); I. Last and M. Baer, *ibid.* **82**, 4954 (1985). For a general discussion see R. D. Levine and R. B. Bernstein, Acc. Chem. Res. **7**, 393 (1974).
[33]M. Baer and H. Nakamura, J. Phys. Chem. (in press).